

A cantilever beam in mass impacting metamaterial for effective vibration control

Muskaan Sethi¹[0000–0002–2437–386X], Arnab Banerjee²[0000–0002–3157–6200],
and Bappaditya Manna²[0000–0003–0739–1035]

¹ Department of Civil Engineering, Indian Institute of Technology, Delhi, India
muskaansethi1106@gmail.com

² Department of Civil Engineering, Indian Institute of Technology, Delhi, India

Abstract. This study presents a novel mass-in-mass metamaterial configuration in which the conventional internal resonator is replaced by a beam. To induce an impacting response, rigid stoppers are introduced on either side of the beam, firmly connected to the primary mass. A time-domain solver is developed based on the linear complementary problem (LCP) formulation and Euler’s discretization to compute the dynamic response of the impacting metamaterial. An experimental investigation is conducted on a beam embedded within a mass-impacting unit cell to validate the LCP solver. The vibration transmission characteristics and effective mass of the proposed unit cell are systematically analyzed, demonstrating the emergence of vibration attenuation band gaps and negative effective mass. These findings underscore the potential of the proposed metamaterial unit cell as a fundamental building block for advanced vibration control systems.

Keywords: linear complementary problem · metamaterial · Euler’s discretization · cantilever beam · transmittance spectrum · effective mass

1 Introduction

The mitigation of vibrations in engineering structures has been an area of significant research interest for several decades [1,2]. Numerous studies have explored various strategies for efficient vibration suppression, including the implementation of tuned liquid dampers [3,4,5], tuned mass dampers [6,7,8], metamaterials [9,10,11], and origami-based metamaterials [12], among others. Among these approaches, metamaterials have drawn particular attention due to their ability to be artificially engineered to achieve desired mechanical properties. By carefully designing their structure and geometry, metamaterials can exhibit unconventional characteristics that are not typically found in natural materials [13,14,15,16,17]. One such property, negative effective mass [17,18,19,20], enables unique control over wave propagation behavior. The ability of metamaterials to generate frequency-dependent effective mass or elasticity plays a crucial role in influencing vibration transmission through these structures [21]. Research indicates that integrating resonators within mechanical metamaterials allows

them to attain these distinct properties [22]. Additionally, such resonators can suppress low-frequency waves without adding extra mass [23,24]. Despite these advantages, a key limitation arises from the fact that their functionality is constrained to narrow frequency ranges due to their reliance on linear resonance [25]. However, this issue can be addressed by leveraging nonlinear metamaterials, as nonlinearity has the potential to broaden the frequency bandwidth in oscillator-based metamaterials.

A linear complementarity approach is commonly employed in contemporary studies to address problems associated with impact and contact mechanics. The multi-body formulation introduced by Moreau [26] and Panagiotopoulos [27,28] established the use of inequality-based impact laws, which can often be reformulated into linear complementarity problem (LCP) frameworks. This approach is particularly effective in modeling unilateral contact conditions [29]. The conventional method involves applying Newton’s impact law in the normal direction [30] and Coulomb’s friction law in the tangential direction [21].

Building upon prior studies that employed impact-based models for vibration attenuation, this work introduces a novel beam-in-mass impacting metamaterial unit cell. The proposed design consists of a cantilever beam enclosed within a rigid mass, functioning as a resonator. When subjected to external excitation, the mass exerts a pseudo force on the cantilever beam, causing it to vibrate. As the beam oscillates, its free end collides with two fixed rigid supports, thereby generating impact events. This paper presents a computational approach based on the LCP framework, coupled with Euler’s discretization, to track variations in the normal gap between the cantilever beam’s free end and the rigid supports over time. The proposed method is validated experimentally and reported in this study.

Following the validation of the proposed numerical scheme, the methodology is further extended to analyze the transmittance spectrum of the beam-in-mass impacting metamaterial unit cell, examining the formation of attenuation bandgaps. Additionally, the effective mass of the unit cell is investigated using a momentum balance approach.

2 LCP based solver for cantilever beam vibrating between two rigid supports

To formulate the LCP based solver for a cantilever beam vibrating between two rigid supports, firstly the dynamic equation of motion for a cantilever beam vibrating between two rigid supports is formulated and presented in subsection 2.1. Further, the formulation of linear complementary equation is explained in subsection 2.2.

2.1 Formulation of dynamic equation of motion for cantilever beam

The contact dynamics for the proposed cantilever beam in mass impacting metamaterial unit cell as shown in Figure 1 have been presented, wherein a vibrating cantilever beam strikes against two rigid supports. The considered cantilever

beam is assumed to be an Euler Bernoulli beam, the dynamic equation for which can be expressed as:

$$EI \frac{\partial^4 w(x, t)}{\partial x^4} + \rho A \frac{\partial^2 w(x, t)}{\partial t^2} = f(x, t) \quad (1)$$

where $w(x, t)$, EI , ρ and A represents the beam deflection in transverse direction, the flexural rigidity of the beam, beam density and the beam cross-sectional area respectively. Further, $f(x, t)$ represents the force acting in the transverse direction at position x on the beam at time t .

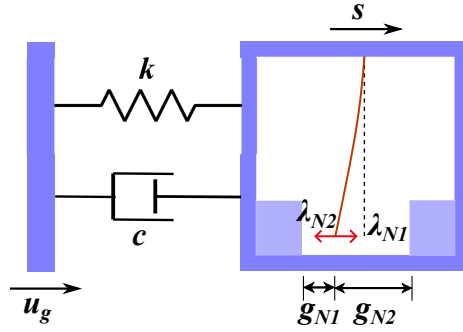


Figure 1. A cantilever flexible beam fixed inside a rigid mass to form an impacting metamaterial unit cell

Equation 1 can be written in discretized form by using Lagrangian equation of motion, as discussed and presented in this section. The solution to Equation 1 can be written as the summation of the product of n number of mode shapes ($\phi_i(x)$) and corresponding time dependent generalized coordinates ($\eta_i(t)$). The higher the number of mode shapes n chosen, the closer would be the solution to the exact solution. Hence, the beam deflection in transverse direction ($w(x, t)$) for the considered cantilever beam is given as [31]:

$$w(x, t) = \sum_{i=1}^n \phi_i(x) \cdot \eta_i(t) \quad (2)$$

where

$$\phi_i(x) = C_n \left[\sin \frac{\beta_i x}{l} - \sinh \frac{\beta_i x}{l} - \alpha_i \left(\cos \frac{\beta_i x}{l} - \cosh \frac{\beta_i x}{l} \right) \right] \quad (3a)$$

where

$$\alpha_i = \left(\frac{\sin \beta_i + \sinh \beta_i}{\cos \beta_i + \cosh \beta_i} \right) \quad (3b)$$

Moreover, β_i can be evaluated by solving the frequency equation given by:

$$\cos \beta_i \cdot \cosh \beta_i = -1 \quad (3c)$$

Furthermore, $\beta_i^2 \left(\frac{EI}{\rho A l^4} \right)^{1/2}$ denotes the natural frequency of the i^{th} mode shape, l represents the length of beam and C_n represents the mass-normalised coefficient of the mode shape.

The expression for potential energy (V) of the beam[31] is given as:

$$V = \frac{1}{2} \int_0^l EI \left(\frac{\partial^2 w}{\partial x^2} \right)^2 dx \quad (4a)$$

$$= \frac{1}{2} \int_0^l EI \left(\sum_{i=1}^n \frac{d^2 \phi_i(x)}{dx^2} \cdot \eta_i(t) \right) \left(\sum_{j=1}^n \frac{d^2 \phi_j(x)}{dx^2} \cdot \eta_j(t) \right) dx \quad (4b)$$

$$= \frac{1}{2} \sum_{i=1}^n \sum_{j=1}^n \underbrace{\int_0^l EI \frac{d^2 \phi_i(x)}{dx^2} \frac{d^2 \phi_j(x)}{dx^2} dx}_{k_{ij}} \eta_i(t) \eta_j(t) \quad (4c)$$

The kinetic energy (T) of the beam[31] can be expressed as:

$$T = \frac{1}{2} \int_0^l \rho A \left(\frac{\partial w}{\partial t} \right)^2 dx \quad (5a)$$

$$= \frac{1}{2} \int_0^l \rho A \left(\sum_{i=1}^n \phi_i(x) \cdot \dot{\eta}_i(t) \right) \left(\sum_{j=1}^n \phi_j(x) \cdot \dot{\eta}_j(t) \right) dx \quad (5b)$$

$$= \frac{1}{2} \sum_{i=1}^n \sum_{j=1}^n \underbrace{\int_0^l \rho A \phi_i(x) \phi_j(x) dx}_{m_{ij}} \dot{\eta}_i(t) \dot{\eta}_j(t) \quad (5c)$$

The expression for work done by non-conservative forces on the beam is written as:

$$\delta W_{NC} = \int_0^l F_{net} \delta w(x, t) dx \quad (6a)$$

$$= \sum_{i=1}^n \int_0^l F_{net} \phi_i(x) \dot{\eta}_i(t) dx \quad (6b)$$

$$= \sum_{i=1}^n \dot{\eta}_i(t) \underbrace{\int_0^l F_{net} \phi_i(x) dx}_{Q_{iNC}} \quad (6c)$$

where F_{net} is the total sum of non-conservative forces acting on the beam, i.e., $F_{net} = [f(x, t) + \{(\lambda_{N1} - \lambda_{N2})\delta_d(x - l)\}]$ and δ_d symbolises the dirac delta function. From the basic understanding of beam dynamics, it is known that

the tip of cantilever beam experiences the maximum deflection when subjected to dynamic loading. Hence, λ_{N1} and λ_{N2} represent the normal reaction forces developed when tip of the cantilever beam strikes the rigid supports.

The Lagrangian equation of motion for the beam is expressed as[31]:

$$\frac{d}{dt} \left(\frac{\partial T}{\partial \dot{\eta}_i} \right) - \frac{\partial T}{\partial \eta_i} + \frac{\partial V}{\partial \eta_i} = Q_{iNC} \quad (7)$$

where $i = 1, 2, 3, \dots, n$. Hence, from Equation 7, n number of equations of motion would be obtained for n generalized coordinates. Substituting the corresponding values in Equation 7 using Equation 4 and Equation 5, the Lagrangian equation of motion takes the form:

$$\sum_{j=1}^n m_{ij} \ddot{\eta}_j(t) + \sum_{j=1}^n k_{ij} \eta_j(t) = Q_{iNC} \quad (8)$$

Moreover, Rayleigh damping can be considered in the beam. Hence, Equation 8 can be re-written as:

$$\sum_{j=1}^n m_{ij} \ddot{\eta}_j(t) + \sum_{j=1}^n k_{ij} \eta_j(t) = Q_{iNC} - \frac{\partial R}{\partial \dot{\eta}_i} \quad (9)$$

where R represents the Rayleigh dissipation function and is given as:

$$R = \frac{1}{2} \sum_{i=1}^n \sum_{j=1}^n c_{ij} \dot{\eta}_i(t) \dot{\eta}_j(t) \quad (10)$$

where c_{ij} represent the damping coefficients, which can be calculated using $c_{ij} = \alpha m_{ij} + \beta k_{ij}$. The value of α and β can be evaluated using the relations, $\alpha = \frac{2\xi\omega_a\omega_b}{\omega_a + \omega_b}$ and $\beta = \frac{2\xi}{\omega_a + \omega_b}$, where ω_a and ω_b are the frequencies of first and fifth mode of vibration respectively [32]. Firstly, the values of mass, stiffness and damping matrices for n^{th} mode are substituted in the expression for Rayleigh damping and the corresponding expression for damping ratio at n^{th} mode is obtained as $\xi_n = \frac{\alpha}{2\omega_n} + \frac{\beta\omega_n}{2}$. Further, by substituting the damping ratios and natural frequencies for first and fifth modes in the aforementioned expression, a set of two simultaneous equations with two unknowns is obtained, which is further solved to get the values of α and β .

Furthermore, Equation 9 can be expressed in the matrix form as:

$$\begin{aligned}
& \underbrace{\begin{bmatrix} m_{11} & m_{12} & \dots & m_{1n} \\ m_{21} & m_{22} & \dots & m_{2n} \\ \vdots & \vdots & \ddots & \vdots \\ m_{n1} & m_{n2} & \dots & m_{nn} \end{bmatrix}}_M \underbrace{\begin{bmatrix} \ddot{\eta}_1 \\ \ddot{\eta}_2 \\ \vdots \\ \ddot{\eta}_n \end{bmatrix}}_{\ddot{u}} - \lambda_{N1} \underbrace{\begin{bmatrix} \phi_1(l) \\ \phi_2(l) \\ \vdots \\ \phi_n(l) \end{bmatrix}}_{W_N} + \lambda_{N2} \underbrace{\begin{bmatrix} \phi_1(l) \\ \phi_2(l) \\ \vdots \\ \phi_n(l) \end{bmatrix}}_{W_N} + \\
& \underbrace{\begin{bmatrix} c_{11} & c_{12} & \dots & c_{1n} \\ c_{21} & c_{22} & \dots & c_{2n} \\ \vdots & \vdots & \ddots & \vdots \\ c_{n1} & c_{n2} & \dots & c_{nn} \end{bmatrix}}_h \underbrace{\begin{bmatrix} \dot{\eta}_1 \\ \dot{\eta}_2 \\ \vdots \\ \dot{\eta}_n \end{bmatrix}}_{\dot{u}} + \underbrace{\begin{bmatrix} k_{11} & k_{12} & \dots & k_{1n} \\ k_{21} & k_{22} & \dots & k_{2n} \\ \vdots & \vdots & \ddots & \vdots \\ k_{n1} & k_{n2} & \dots & k_{nn} \end{bmatrix}}_{-h} \underbrace{\begin{bmatrix} \eta_1 \\ \eta_2 \\ \vdots \\ \eta_n \end{bmatrix}}_{\eta} - \underbrace{\begin{bmatrix} f_1(x, t) \\ f_2(x, t) \\ \vdots \\ f_n(x, t) \end{bmatrix}}_{f} = \begin{bmatrix} 0 \\ 0 \\ \vdots \\ 0 \end{bmatrix} \quad (11)
\end{aligned}$$

and $f_i(x, t) = \int_0^l f(x, t) \cdot \phi_i(x) dx$. Therefore, Equation 11 takes the form of general equation of motion written at acceleration level for dynamic systems with normal forces, and expressed as:

$$M\ddot{u} - h - W_N\lambda_{N1} + W_N\lambda_{N2} = 0 \quad (12)$$

where M represents the mass matrix, h represents the force vector and W_N represents the normal directional matrix. Substituting $\ddot{u} = \Delta q / \Delta t$ and applying Euler's discretization to Equation 12, we get:

$$M\Delta q - h\Delta t - W_N\Lambda_{N1} + W_N\Lambda_{N2} = 0 \quad (13a)$$

$$\Delta q = M^{-1}(h\Delta t + W_N\Lambda_{N1} - W_N\Lambda_{N2}) \quad (13b)$$

$$\Delta u = (q + \Delta q)\Delta t \quad (13c)$$

$$\Delta u = [q + M^{-1}(h\Delta t + W_N\Lambda_{N1} - W_N\Lambda_{N2})]\Delta t \quad (13d)$$

where $q = \dot{u}$ and $\Lambda_k = \lambda_k \Delta t$, where $k = 1, 2$.

2.2 Formulation of LCP equation for a vibrating cantilever beam hitting against rigid supports

The Linear Complementary Problem (LCP) approach can be adopted to solve the dynamics of contact or impact problems. Generally, the LCP equations are of the form: $y = Ax + B$, such that $y \geq 0$, $x \geq 0$ and $x^T y = 0$ i.e. the complementary condition.

This paper deals with the application of LCP approach to investigate various cantilever systems in which the tip of cantilever beam strikes against rigid supports, as shown in Figure 1. g_{N1} and g_{N2} represent the normal gap from the tip of cantilever beam to rigid support-1 and rigid support-2 respectively. The normal gaps g_{N1} and g_{N2} and normal reaction forces λ_{N1} and λ_{N2} form the complementary conditions, i.e. $g_{N1} \cdot \lambda_{N1} = 0$ and $g_{N2} \cdot \lambda_{N2} = 0$, as the normal

reaction forces will be non-zero when corresponding normal gaps are zero and vice-versa. Applying Taylor series expansion to normal gaps (g_{N1} and g_{N2}) and ignoring higher order terms of Δu and Δt yields:

$$g_{N1}^e = g_{N1} + \Delta g_{N1}(u, t) = g_{N1} + \underbrace{\frac{\partial g_{N1}}{\partial u}}_{X_{N1}^T} \Delta u + \underbrace{\frac{\partial g_{N1}}{\partial t}}_{\tilde{w}_{N1}} \Delta t \quad (14)$$

$$g_{N2}^e = g_{N2} + \Delta g_{N2}(u, t) = g_{N2} + \underbrace{\frac{\partial g_{N2}}{\partial u}}_{X_{N2}^T} \Delta u + \underbrace{\frac{\partial g_{N2}}{\partial t}}_{\tilde{w}_{N2}} \Delta t \quad (15)$$

where u represents the vector of generalised coordinates, $X_{N1} = \left(\frac{\partial g_{N1}}{\partial u}\right)^T$, $X_{N2} = \left(\frac{\partial g_{N2}}{\partial u}\right)^T$, $\tilde{w}_{N1} = \left(\frac{\partial g_{N1}}{\partial t}\right)$ and $\tilde{w}_{N2} = \left(\frac{\partial g_{N2}}{\partial t}\right)$. The superscript e is used to denote the corresponding value at the end of time step. Eliminating the value of Δu from Equation 14 and Equation 15 using Equation 13(d), the following is obtained:

$$\begin{aligned} g_{N1}^e &= g_{N1} + X_{N1}^T [q + M^{-1}(h\Delta t + W_N \Lambda_{N1} - W_N \Lambda_{N2})] \Delta t + \tilde{w}_{N1} \Delta t \\ &= \underbrace{X_{N1}^T M^{-1} W_N \Lambda_{N1} \Delta t}_{G_{XN1}} - \underbrace{X_{N1}^T M^{-1} W_N \Lambda_{N2} \Delta t}_{G_{XN1}} + \\ &\quad \underbrace{X_{N1}^T (q + M^{-1} h \Delta t) \Delta t + g_{N1} + \tilde{w}_{N1} \Delta t}_{C_{N1}} \end{aligned} \quad (16)$$

$$\begin{aligned} g_{N2}^e &= g_{N2} + X_{N2}^T [q + M^{-1}(h\Delta t + W_N \Lambda_{N1} - W_N \Lambda_{N2})] \Delta t + \tilde{w}_{N2} \Delta t \\ &= \underbrace{X_{N2}^T M^{-1} W_N \Lambda_{N1} \Delta t}_{G_{XN2}} - \underbrace{X_{N2}^T M^{-1} W_N \Lambda_{N2} \Delta t}_{G_{XN2}} + \\ &\quad \underbrace{X_{N2}^T (q + M^{-1} h \Delta t) \Delta t + g_{N2} + \tilde{w}_{N2} \Delta t}_{C_{N2}} \end{aligned} \quad (17)$$

Hence, using Equation 16 and Equation 17 the final LCP equation can be written as:

$$\begin{bmatrix} g_{N1}^e \\ g_{N2}^e \end{bmatrix} = \begin{bmatrix} G_{XN1} \Delta t & -G_{XN1} \Delta t \\ G_{XN2} \Delta t & -G_{XN2} \Delta t \end{bmatrix} \begin{bmatrix} \Lambda_{N1} \\ \Lambda_{N2} \end{bmatrix} + \begin{bmatrix} C_{N1} \\ C_{N2} \end{bmatrix} \quad (18)$$

Further, the expressions for normal gaps can be written as:

$$\begin{aligned} g_{N1} &= g_1 + w(l, t) = g_1 + W_N^T u \\ g_{N2} &= g_2 - w(l, t) = g_2 - W_N^T u \end{aligned} \quad (19)$$

By differentiating the above equations, we get:

$$\begin{aligned} \Delta g_{N1} &= W_N^T \Delta u \\ \Delta g_{N2} &= -W_N^T \Delta u \end{aligned} \quad (20)$$

Comparing the above equations with the terms in Equation 14 and Equation 15, we get $X_{N1} = W_N, \tilde{\omega}_{N1} = 0, X_{N2} = -W_N$ and $\tilde{\omega}_{N2} = 0$.

The LCP equation in Equation 18 can be solved at each time step using various algorithms, like Lemke's algorithm used in present study. The solution thus obtained gives the values of normal reaction impulses λ_{N1} and λ_{N2} , which can be then used in Equation 13 to calculate the system state at the next time step. The solver has been expressed using a flow chart in Figure 2 and various simulations are run using MATLAB software.

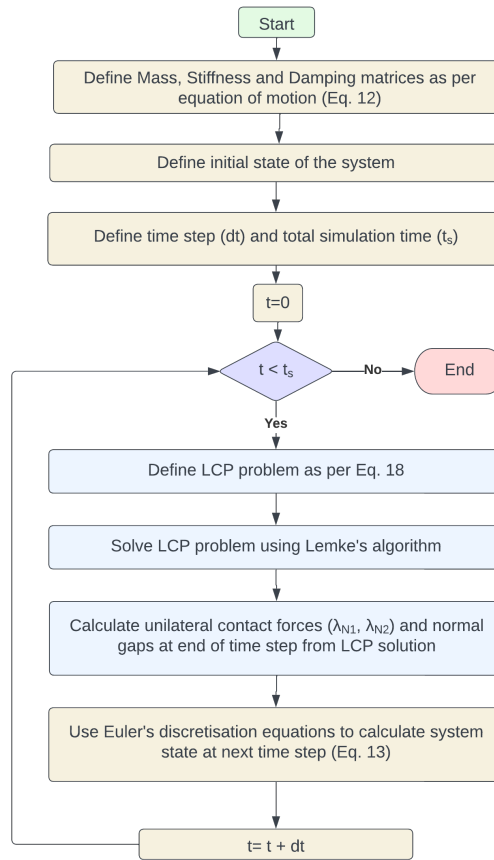


Figure 2. Flow chart depicting the LCP based solver.

3 A cantilever beam in mass impacting metamaterial unit cell

A metamaterial unit cell formed by fixing a cantilever beam inside a rigid mass is considered as shown in Figure 1. In such a metamaterial unit cell, the cantilever beam behaves like a resonator and vibrates between two rigid supports when the outer mass is given an external excitation.

To formulate the LCP equation for this proposed metamaterial unit cell, the required parameters are given as:

$$\begin{aligned} f(x, t) &= \rho A \ddot{s} \\ Q_{iNC} &= \int_0^l [\rho A \ddot{s} + \{(-\lambda_{N1} + \lambda_{N2})\delta_d(x - l)\}] \phi_i(x) \end{aligned} \quad (21)$$

where s represents displacement in the outer mass, ρA represents the mass per unit length of the beam and $\rho A \ddot{s}$ represents the inertial force developed on the cantilever beam due to motion of the outer mass.

Hence, by substituting Q_{iNC} in Equation 9 the equation of motion for the cantilever beam is expressed as:

$$\begin{aligned} \sum_{j=1}^n m_{ij} \ddot{\eta}_j(t) + \sum_{j=1}^n c_{ij} \dot{\eta}_j(t) + \sum_{j=1}^n k_{ij} \eta_j(t) - \\ \int_0^l \rho A \ddot{s} \phi_i(x) dx = (-\lambda_{N1} + \lambda_{N2}) \cdot \phi_i(l) \end{aligned} \quad (22)$$

Moreover, the equation of motion for the outer rigid mass can be expressed as:

$$m_o \ddot{s} = -\lambda_{N1} + \lambda_{N2} - k(s - u_g) - c(\dot{s} - \dot{u}_g) \quad (23)$$

Therefore, the combined equation of motion for the cantilever beam and outer mass in the considered metamaterial unit cell would be given as:

$$\begin{aligned}
& \begin{bmatrix} m_{11} & m_{12} & \dots & m_{1n} & -\int_0^l \rho A \phi_1(x) dx \\ m_{21} & m_{22} & \dots & m_{2n} & -\int_0^l \rho A \phi_2(x) dx \\ \vdots & \vdots & \vdots & \vdots & \vdots \\ m_{n1} & m_{n2} & \dots & m_{nn} & -\int_0^l \rho A \phi_n(x) dx \\ 0 & 0 & \dots & 0 & m_o \end{bmatrix} \begin{bmatrix} \ddot{\eta}_1 \\ \ddot{\eta}_2 \\ \vdots \\ \ddot{\eta}_n \\ \ddot{s} \end{bmatrix} + \begin{bmatrix} c_{11} & c_{12} & \dots & c_{1n} & 0 \\ c_{21} & c_{22} & \dots & c_{2n} & 0 \\ \vdots & \vdots & \vdots & \vdots & \vdots \\ c_{n1} & c_{n2} & \dots & c_{nn} & 0 \\ 0 & 0 & \dots & 0 & c \end{bmatrix} \begin{bmatrix} \dot{\eta}_1 \\ \dot{\eta}_2 \\ \vdots \\ \dot{\eta}_n \\ \dot{s} \end{bmatrix} + \\
& \begin{bmatrix} k_{11} & k_{12} & \dots & k_{1n} & 0 \\ k_{21} & k_{22} & \dots & k_{2n} & 0 \\ \vdots & \vdots & \vdots & \vdots & \vdots \\ k_{n1} & k_{n2} & \dots & k_{nn} & 0 \\ 0 & 0 & \dots & 0 & k \end{bmatrix} \begin{bmatrix} \eta_1 \\ \eta_2 \\ \vdots \\ \eta_n \\ s \end{bmatrix} - \lambda_{N1} \begin{bmatrix} -\phi_1(l) \\ -\phi_2(l) \\ \vdots \\ -\phi_n(l) \\ -1 \end{bmatrix} - \\
& \lambda_{N2} \begin{bmatrix} \phi_1(l) \\ \phi_2(l) \\ \vdots \\ \phi_n(l) \\ 1 \end{bmatrix} - \begin{bmatrix} 0 \\ 0 \\ \vdots \\ 0 \\ k u_g + c \dot{u}_g \end{bmatrix} = \begin{bmatrix} 0 \\ 0 \\ \vdots \\ 0 \\ 0 \end{bmatrix} \tag{24}
\end{aligned}$$

where u_g and \dot{u}_g represents the ground excitation displacement and velocity respectively which can be expressed as:

$$u_g = U_g \sin \bar{\omega} t \implies \dot{u}_g = U_g \bar{\omega} \cos \bar{\omega} t \tag{25}$$

Equation 24 can be non-dimensionalized by using the following parameters:

$$\begin{aligned}
k &= m_o \omega_m^2; \quad c = 2\xi \omega_m m_o; \quad \eta_i = B \tilde{\eta}_i; \quad s = B \tilde{s}; \\
\lambda_{N1} &= N \tilde{\lambda}_{N1}; \quad \lambda_{N2} = N \tilde{\lambda}_{N2}; \quad t = \frac{\tau}{\omega_b}
\end{aligned} \tag{26}$$

Therefore, Equation 24 can be written as:

$$\begin{aligned}
& \rho Al \begin{bmatrix} a_{11} & a_{12} & \dots & a_{1n} & -d_1 \\ a_{21} & a_{22} & \dots & a_{2n} & -d_2 \\ \vdots & \vdots & \vdots & \vdots & \vdots \\ a_{n1} & a_{n2} & \dots & a_{nn} & -d_n \\ 0 & 0 & \dots & 0 & \frac{m_o}{\rho Al} \end{bmatrix} \begin{bmatrix} \omega_b^2 B \ddot{\eta}_1 \\ \omega_b^2 B \ddot{\eta}_2 \\ \vdots \\ \omega_b^2 B \ddot{\eta}_n \\ \omega_b^2 B \ddot{s} \end{bmatrix} + \begin{bmatrix} c_{11} & c_{12} & \dots & c_{1n} & 0 \\ c_{21} & c_{22} & \dots & c_{2n} & 0 \\ \vdots & \vdots & \vdots & \vdots & \vdots \\ c_{n1} & c_{n2} & \dots & c_{nn} & 0 \\ 0 & 0 & \dots & 0 & 2\xi\omega_m m_o \end{bmatrix} \begin{bmatrix} \omega_b B \dot{\eta}_1 \\ \omega_b B \dot{\eta}_2 \\ \vdots \\ \omega_b B \dot{\eta}_n \\ \omega_b B \dot{s} \end{bmatrix} + \\
& \begin{bmatrix} \left(\frac{EI}{l^3}\right) b_{11} & \left(\frac{EI}{l^3}\right) b_{12} & \dots & \left(\frac{EI}{l^3}\right) b_{1n} & 0 \\ \left(\frac{EI}{l^3}\right) b_{21} & \left(\frac{EI}{l^3}\right) b_{22} & \dots & \left(\frac{EI}{l^3}\right) b_{2n} & 0 \\ \vdots & \vdots & \vdots & \vdots & \vdots \\ \left(\frac{EI}{l^3}\right) b_{n1} & \left(\frac{EI}{l^3}\right) b_{n2} & \dots & \left(\frac{EI}{l^3}\right) b_{nn} & 0 \\ 0 & 0 & \dots & 0 & m_o \omega_m^2 \end{bmatrix} \begin{bmatrix} B \tilde{\eta}_1 \\ B \tilde{\eta}_2 \\ \vdots \\ B \tilde{\eta}_n \\ B \tilde{s} \end{bmatrix} - N \tilde{\lambda}_{N1} \begin{bmatrix} -\phi_1(l) \\ -\phi_2(l) \\ \vdots \\ -\phi_n(l) \\ -1 \end{bmatrix} - \\
& N \tilde{\lambda}_{N2} \begin{bmatrix} \phi_1(l) \\ \phi_2(l) \\ \vdots \\ \phi_n(l) \\ 1 \end{bmatrix} - \begin{bmatrix} 0 \\ 0 \\ \vdots \\ 0 \\ \left(m_o \omega_m^2 U_g \sin \frac{\bar{\omega}\tau}{\omega_b}\right) + \left(2\xi\omega_m m_o U_g \bar{\omega} \cos \frac{\bar{\omega}\tau}{\omega_b}\right) \end{bmatrix} = \begin{bmatrix} 0 \\ 0 \\ \vdots \\ 0 \\ 0 \end{bmatrix} \quad (27)
\end{aligned}$$

where

$$\begin{aligned}
a_{ij} &= \int_0^1 \phi_i(lx_1) \cdot \phi_j(lx_1) dx_1, \quad b_{ij} = \int_0^1 \frac{d^2 \phi_i(lx_1)}{dx_1^2} \cdot \frac{d^2 \phi_j(lx_1)}{dx_1^2} dx_1, \\
d_i &= \int_0^1 \phi_i(lx_1) dx_1.
\end{aligned} \quad (28)$$

These coefficients are obtained by non-dimensionalization of m_{ij} , k_{ij} and $\int_0^l \rho A \phi_i(x) dx$ respectively by substituting $x = lx_1$ in their corresponding expressions. Moreover, ω_m represent the natural frequency of the mass and ω_b is a parameter used for non dimensionalization.

The final non-dimensional form of Equation 27 can be expressed as:

$$\begin{aligned}
& \underbrace{\begin{bmatrix} a_{11} & a_{12} & \dots & a_{1n} & -d_1 \\ a_{21} & a_{22} & \dots & a_{2n} & -d_2 \\ \vdots & \vdots & \vdots & \vdots & \vdots \\ a_{n1} & a_{n2} & \dots & a_{nn} & -d_n \\ 0 & 0 & \dots & 0 & \frac{1}{\theta} \end{bmatrix}}_{\tilde{M}} \underbrace{\begin{bmatrix} \ddot{\tilde{\eta}}_1 \\ \ddot{\tilde{\eta}}_2 \\ \vdots \\ \ddot{\tilde{\eta}}_n \\ \ddot{\tilde{s}} \end{bmatrix}}_{\ddot{\tilde{u}}} + \underbrace{\begin{bmatrix} \tilde{c}_{11} & \tilde{c}_{12} & \dots & \tilde{c}_{1n} & 0 \\ \tilde{c}_{21} & \tilde{c}_{22} & \dots & \tilde{c}_{2n} & 0 \\ \vdots & \vdots & \vdots & \vdots & \vdots \\ \tilde{c}_{n1} & \tilde{c}_{n2} & \dots & \tilde{c}_{nn} & 0 \\ 0 & 0 & \dots & 0 & \frac{2\xi}{\theta\gamma_s} \end{bmatrix}}_{\tilde{C}} \underbrace{\begin{bmatrix} \dot{\tilde{\eta}}_1 \\ \dot{\tilde{\eta}}_2 \\ \vdots \\ \dot{\tilde{\eta}}_n \\ \dot{\tilde{s}} \end{bmatrix}}_{\dot{\tilde{u}}} + \\
& \underbrace{\begin{bmatrix} \sigma b_{11} & \sigma b_{12} & \dots & \sigma b_{1n} & 0 \\ \sigma b_{21} & \sigma b_{22} & \dots & \sigma b_{2n} & 0 \\ \vdots & \vdots & \vdots & \vdots & \vdots \\ \sigma b_{n1} & \sigma b_{n2} & \dots & \sigma b_{nn} & 0 \\ 0 & 0 & \dots & 0 & \frac{1}{\theta\gamma_s^2} \end{bmatrix}}_{\tilde{K}} \underbrace{\begin{bmatrix} \tilde{\eta}_1 \\ \tilde{\eta}_2 \\ \vdots \\ \tilde{\eta}_n \\ \tilde{s} \end{bmatrix}}_{\tilde{u}} + \tilde{\lambda}_{N1} \underbrace{\begin{bmatrix} \phi_1(l) \\ \phi_2(l) \\ \vdots \\ \phi_n(l) \\ 1 \end{bmatrix}}_{X_N} - \tilde{\lambda}_{N2} \underbrace{\begin{bmatrix} \phi_1(l) \\ \phi_2(l) \\ \vdots \\ \phi_n(l) \\ 1 \end{bmatrix}}_{X_N} - \\
& \underbrace{\begin{bmatrix} 0 \\ 0 \\ \vdots \\ 0 \\ \frac{1}{\gamma_s} \sin \gamma_r \tau + 2\xi \gamma_r \cos \gamma_r \tau \end{bmatrix}}_{\tilde{F}} = \begin{bmatrix} 0 \\ 0 \\ \vdots \\ 0 \\ 0 \end{bmatrix} \quad (29)
\end{aligned}$$

where

$$\frac{1}{\theta} = \frac{m_o}{\rho Al}, \quad \gamma_s = \frac{\omega_b}{\omega_m}, \quad \gamma_r = \frac{\bar{\omega}}{\omega_b}, \quad \sigma = \frac{EI}{\rho Al^4 \omega_b^2}, \quad U_g = B\theta\gamma_s, \quad N = \rho Al B \omega_b^2 \quad (30)$$

θ represents the mass ratio, γ_r represents the non dimensional excitation frequency, γ_s represents the inverse of natural frequency of outer mass, \tilde{c}_{ij} represents the non-dimensional damping coefficients, ξ represents the damping ratio, B is an arbitrary constant and U_g is the amplitude of excitation.

Hence, Equation 29 is similar to the form given in Equation 12, such that $W_N = X_N$ and $h = \tilde{h} = -\tilde{C}\dot{\tilde{u}} - \tilde{K}\tilde{u} + \tilde{F}$. Moreover, $\tilde{M}, \tilde{C}, \tilde{K}$ and \tilde{F} are the non-dimensional mass matrix, damping matrix, stiffness matrix and force vector respectively.

Therefore, to write the final LCP equation in non-dimensional form, substitute $g_{N1} = B\tilde{g}_{N1}, g_{N2} = B\tilde{g}_{N2}$ and $\Delta u = B\Delta\tilde{u}$ in Equation 18, the final non-dimensional LCP equation for this case is expressed as:

$$\begin{bmatrix} \tilde{g}_{N1}^e \\ \tilde{g}_{N2}^e \end{bmatrix} = \begin{bmatrix} \tilde{G}_{XN}\Delta\tau & -\tilde{G}_{XN}\Delta\tau \\ -\tilde{G}_{XN}\Delta\tau & \tilde{G}_{XN}\Delta\tau \end{bmatrix} \begin{bmatrix} \tilde{A}_{N1} \\ \tilde{A}_{N2} \end{bmatrix} + \begin{bmatrix} \tilde{C}_{N1} \\ \tilde{C}_{N2} \end{bmatrix} \quad (31)$$

where $\tilde{G}_{XN} = W_N^T \tilde{M}^{-1} X_N$, $\tilde{C}_{N1} = -W_N^T (\tilde{q} + \tilde{M}^{-1} \tilde{h} \Delta\tau) \Delta\tau + \tilde{g}_{N1}$, $\tilde{C}_{N2} = W_N^T (\tilde{q} + \tilde{M}^{-1} \tilde{h} \Delta\tau) \Delta\tau + \tilde{g}_{N2}$. Moreover, \tilde{g}_{N1} and \tilde{g}_{N2} represent the non-dimensional normal gaps.

Further, the transmittance in the outer mass can be calculated as:

$$\Gamma = 20 \log_{10} \left| \frac{s}{u_g} \right| = 20 \log_{10} \left| \frac{B\tilde{s}}{U_g} \right| = 20 \log_{10} \left| \frac{\tilde{s}}{\theta\gamma_s} \right| \quad (32)$$

A comprehensive analysis of the transmittance spectrum is presented in section 4 to examine both the quantitative and qualitative characteristics of the bandgaps in the proposed metamaterial unit cell. Due to the presence of non-linear impact forces in the unit cell, conventional analytical techniques such as the Transfer Matrix Method or eigenvalue solutions using Bloch’s theorem are not suitable for accurately capturing its behavior. As a result, deriving a closed-form solution for analytical bandgap analysis becomes challenging. To address this, the present study employs the transmittance spectrum as an effective approach for bandgap investigation. Previous studies [33,34,35] have successfully utilized transmittance spectrum analysis for bandgap studies, demonstrating strong agreement with dispersion curve-based methods.

4 Results and Discussion

First, the experimental validation of the proposed solver for the cantilever beam in mass metamaterial unit cell is presented in subsection 4.1.

The transmittance spectrum of a cantilever beam in mass metamaterial unit cell is analyzed and plotted for different parameters. Additionally, the effective mass is calculated and visualized using the momentum balance approach.

4.1 Experimental validation of the proposed solver for the metamaterial unit cell

To provide a more comprehensive validation of the proposed LCP solver with experimental results, an experiment was conducted to analyze the transmittance spectrum of a cantilever beam in mass impacting metamaterial. The details of this study are discussed and presented in this section.

Experimental Setup A cantilever beam in mass impacting metamaterial unit cell was fabricated using PLA material with a 3D printer. The unit cell is connected to the shaker system via a spring with a stiffness coefficient of 350 N/m , as illustrated in Figure 3(a). To reduce frictional effects, a layer of oil is applied between the unit cell and the surface. Furthermore, the unit cell rests on four hemispherical contact points at the corners, minimizing its contact area with the base surface. Two triaxial accelerometers are mounted—one for capturing the base excitation data and the other for measuring vibrations within the unit cell, as shown in Figure 3(b). The parameters of the unit cell are provided in Table 1. Additionally, the mass of the accelerometer attached to the unit cell is included in the outer mass.

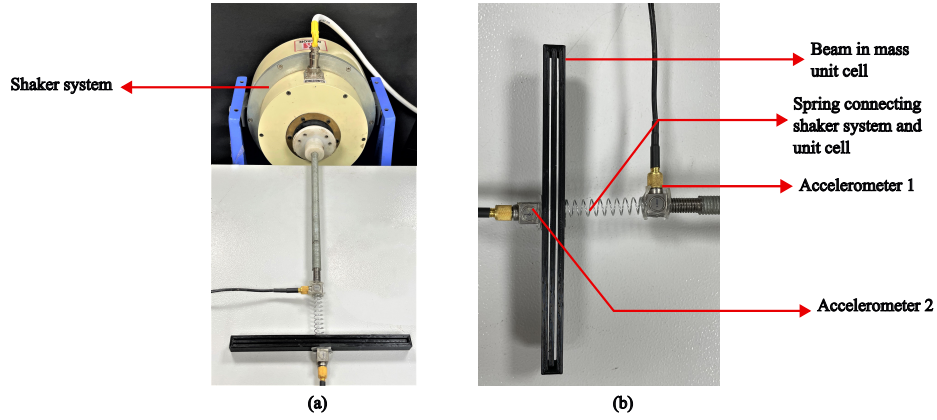


Figure 3. Experimental setup to validate the proposed LCP solver for transmittance spectrum of a cantilever beam in mass impacting metamaterial unit cell (a) Complete setup showing the proposed unit cell connected to shaker system (b) Enlarged view of the unit cell with attached accelerometers.

Table 1. Unit cell parameters

Unit cell Parameter	Value
Material	Polylactic acid (PLA)
Length of beam	0.15 <i>m</i>
Breadth of beam	0.01 <i>m</i>
Thickness of beam	0.0025 <i>m</i>
Gap between beam and outer mass	0.001 <i>m</i>
Density of unit cell	1250 <i>kg/m</i> ³
Young's Modulus (<i>E</i>)	4.583 × 10 ⁷ <i>N/m</i> ²
Outer mass	12.67 <i>g</i>
Mass of accelerometer	4 <i>g</i>

Experimental methodology The experiment is conducted by configuring the frequency and gain of the shaker system and collecting data from the accelerometers using Labview software at a sampling rate of 500 *samples/second* for 10 seconds. Data was recorded for excitation frequency values ranging from 12*Hz* to 22*Hz* in increments of 2*Hz*, from 23*Hz* to 30*Hz* in increments of 1*Hz*, and from 32*Hz* to 42*Hz* in increments of 2*Hz*. The base excitation u_g for the analytical study is obtained by converting the time-series data recorded from the accelerometer attached to the base plate into the frequency domain using the Fourier transform. The physical parameters listed in Table 1, along with the derived base excitation function, are then utilized in the analytical study using the solver with physical parameters as per Equation 24. Additionally, the experiment was repeated three times to obtain three sets of data.

Validation of proposed solver with experimental results The data from the accelerometer attached to the base of shaker system is used to find the amplitude of base excitation, which is then used in the analytical solver. The transmittance in the unit cell is calculated as below:

$$\Gamma = 20 \log_{10} \left| \frac{x}{U_g} \right| \quad (33)$$

where, x is the amplitude of induced vibrations in the unit cell and U_g is the amplitude of base excitation. The analytical solver results, along with three sets of experimental data, are presented in Figure 4. It is evident that the analytical predictions align well with the experimental findings. The slight discrepancies observed at lower frequencies can be attributed to the higher error tolerance in the accelerometer's sensitivity at lower frequency ranges, as indicated in its calibration certificate. Furthermore, experimental errors may also arise due to the resistance introduced by the accelerometer wire attached to the unit cell. Overall, the experimental validation provides strong confidence in the accuracy of the proposed LCP-based solver.

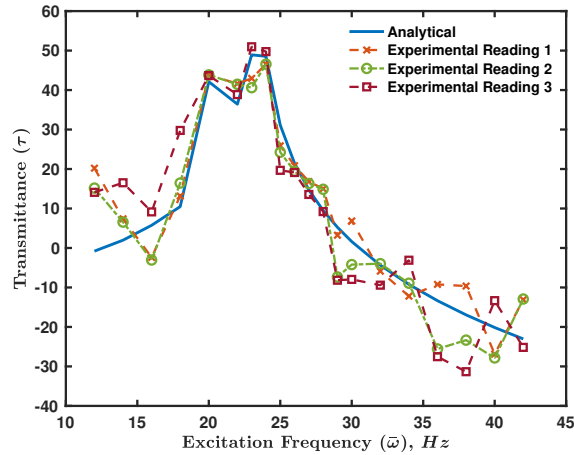


Figure 4. Transmittance plot for a beam in mass impacting unit cell comparing results obtained from the LCP based solver and that from three readings from experimental study.

4.2 Transmittance spectrum for metamaterial unit cell

From the formulation of final LCP equation for the considered unit cell, it is observed that the response of such a system depends on the non-dimensional

gaps (\tilde{g}_1, \tilde{g}_2), mass ratio (θ), inverse of natural frequency of outer mass (γ_s) and stiffness parameter of inner beam (σ). Hence, the transmittance plots with respect to varying non dimensional excitation frequency (γ_r) are plotted for different values of these parameters using the solver developed in MATLAB. The following observations are perceived:

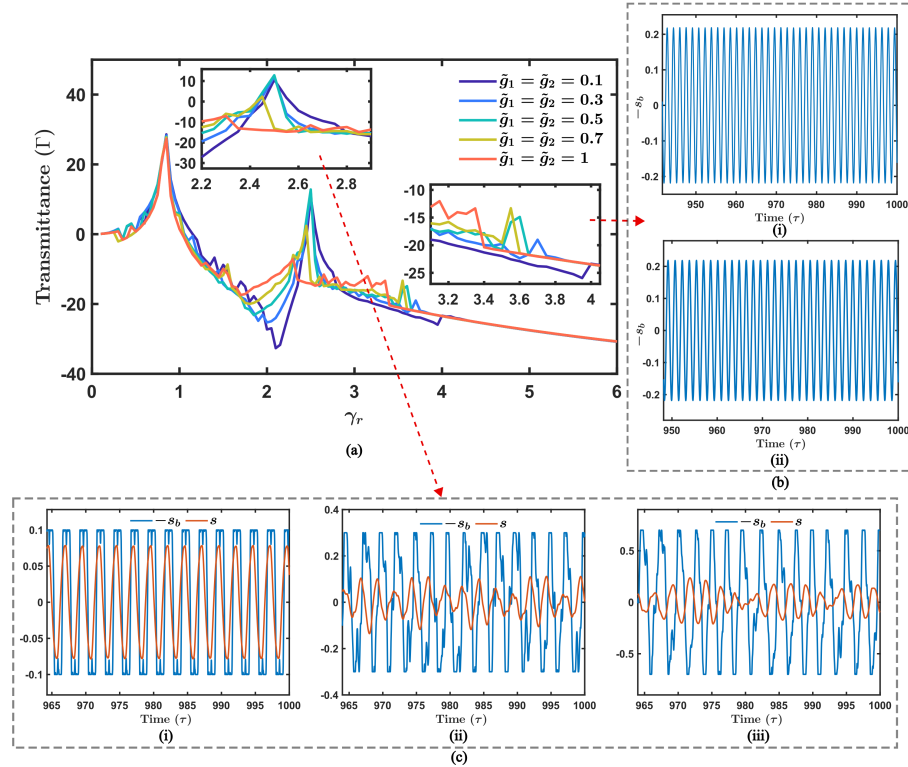


Figure 5. (a) Transmittance with respect to varying non dimensional excitation frequency (γ_r) for different values of non-dimensional normal gaps (\tilde{g}_1, \tilde{g}_2), (b) Time history plots of non dimensional tip displacement of inner beam ($-s_b$) for $\gamma_r = 4$ and (i) $\tilde{g}_1 = \tilde{g}_2 = 0.5$ and (ii) $\tilde{g}_1 = \tilde{g}_2 = 1$, and (c) Time history plots of non dimensional tip displacement of inner beam ($-s_b$) and displacement of outer mass (\bar{s}) for $\gamma_r = 2.5$ and (i) $\tilde{g}_1 = \tilde{g}_2 = 0.1$, (ii) $\tilde{g}_1 = \tilde{g}_2 = 0.3$ and (iii) $\tilde{g}_1 = \tilde{g}_2 = 0.7$

- Figure 5(a) illustrates the variation in transmittance of the outer mass for different values of non-dimensional normal gaps (\tilde{g}_1, \tilde{g}_2) between the beam tip and the outer mass. It can be observed from Figure 5(a) that a second propagation band appears for γ_r in the range of 2.2 to 3. Additionally, the peak transmittance decreases progressively as the values of \tilde{g}_1 and \tilde{g}_2 increase. This trend is further explained by the time history plots in Figure 5(c). When

- the normal gap is relatively small, specifically $\tilde{g}_1 = \tilde{g}_2 = 0.1$, the displacement of the beam tip remains in phase with the displacement of the outer mass, as shown in Figure 5(c-i). Consequently, the impact force enhances the displacement of the outer mass, leading to an increase in transmittance. Conversely, as the normal gap values increase, the beam tip displacement and the displacement of the outer mass gradually shift out of phase, as depicted in Figure 5(c-ii) and Figure 5(c-iii). This phase mismatch reduces the displacement of the outer mass, thereby lowering the transmittance value.
- Furthermore, as observed in Figure 5(a), beyond a certain high-frequency threshold, the beam tip ceases to impact the outer mass. The excitation frequency at which this phenomenon occurs is lower for larger values of the normal gap. Consequently, beyond this point, variations in the normal gap no longer influence the transmittance behavior, causing the different plots to converge into a straight line. This observation is further corroborated by the time history plots in Figure 5(b), which show that for different normal gap values, the peak displacement of the beam tip remains nearly identical. This clearly indicates that the effect of varying normal gaps diminishes beyond a specific frequency.
 - Additionally, it is observed that the anti-resonance drop is more pronounced for smaller normal gap values compared to larger ones. This occurs because, at that frequency, the outer mass and the vibrating beam move out of phase with each other. To sustain the same vibration frequency in steady-state conditions, a smaller normal gap results in a longer impact duration compared to a larger gap. Consequently, the displacement of the outer mass decreases, leading to a reduction in transmittance.

4.3 Effective mass of metamaterial unit cell

An average effective mass can be computed for the cantilever beam in mass impacting metamaterial unit cell by the concept of momentum balance, described as below:

$$M_{eff}\dot{s} = m_o\dot{s} - \int_0^l \rho A \sum_{i=1}^n \phi_i(x)\dot{\eta}_i(t)dx = m_o\dot{s} - \int_0^1 \rho Al \sum_{i=1}^n \phi_i(lx_1)\dot{\eta}_i(t)dx_1 \quad (34a)$$

$$M_{eff} = m_o - \underbrace{\frac{\rho Al}{\dot{s}} \sum_{i=1}^n \int_0^1 \phi_i(lx_1)\dot{\eta}_i(dx_1)}_{\dot{s}_b} = m_o - \frac{\rho Al}{\dot{s}}\dot{s}_b \quad (34b)$$

$$\theta_{eff} = \frac{M_{eff}}{m_o + \rho Al} = \frac{M_{eff}/m_o}{1 + \theta} \quad (35)$$

Substituting the value of M_{eff} from Equation 34b to Equation 35, the final expression for θ_{eff} is obtained as:

$$\theta_{eff} = \frac{1 - \theta \left(\frac{\dot{s}_b}{\dot{s}} \right)}{1 + \theta} \quad (36)$$

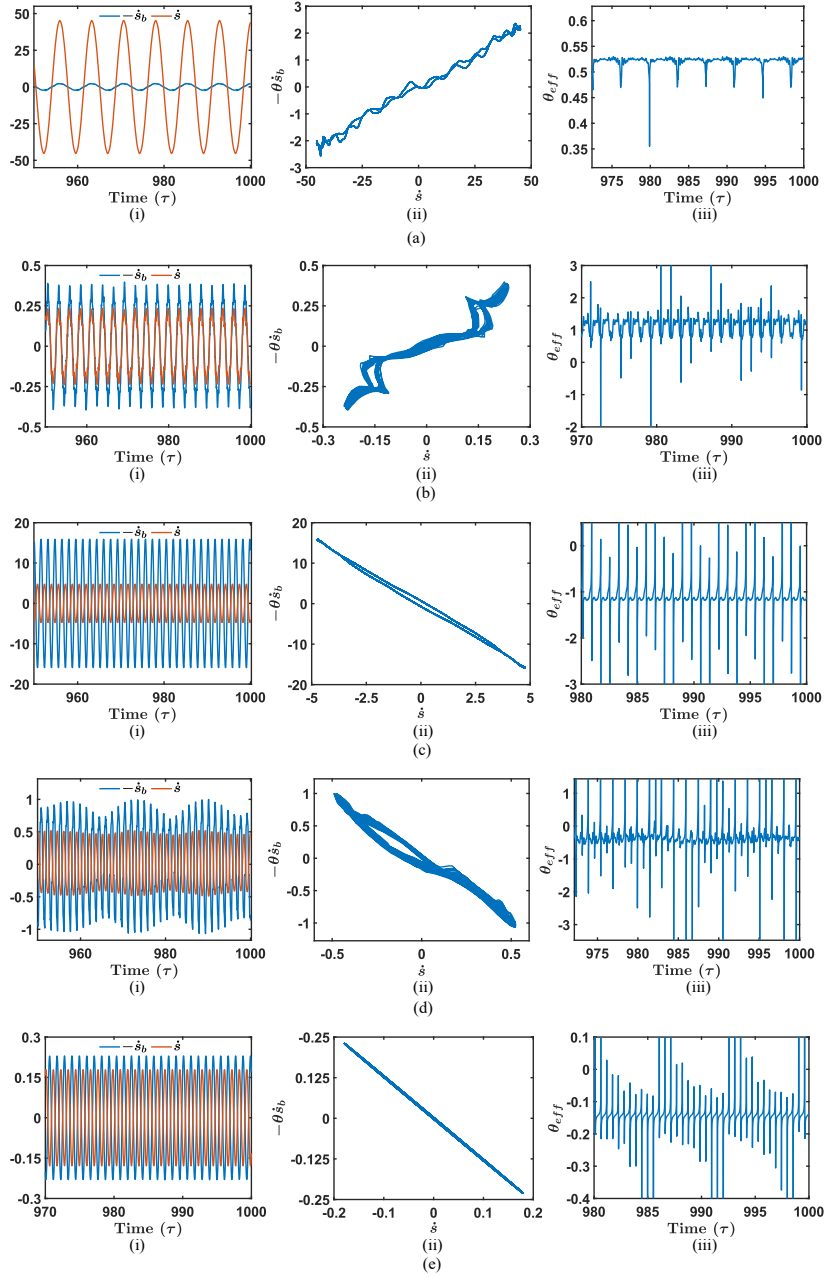


Figure 6. Study of negative effective mass property of the proposed metamaterial unit cell. (i) Time history plots for velocity of outer mass (\dot{s}) and inner beam tip ($-\dot{s}_b$) (ii) Phase portrait for varying $-\theta\dot{s}_b$ with respect to \dot{s} (iii) Time history plot for variation of θ_{eff} for (a) $\gamma_r = 0.85$ (b) $\gamma_r = 2.35$ (c) $\gamma_r = 3.9$ (d) $\gamma_r = 4.15$ (e) $\gamma_r = 5.8$

Figure 6 illustrates the time history plots for the velocity of the outer mass (\dot{s}) and the inner beam ($-\dot{s}_b$), the phase portrait depicting the variation of $-\theta\dot{s}_b$ with respect to \dot{s} , and the time history plot showing the variation of θ_{eff} for different values of γ_r , while maintaining $\gamma_s = 1$, $\sigma = 0.05$, and $\tilde{g}_1 = \tilde{g}_2 = 0.1$. The following observations are obtained:

- The time history plots in Figure 6(a-i) and Figure 6(b-i) illustrate that the motion of the beam and the outer mass remains in phase. Consequently, the corresponding phase portrait plots in Figure 6(a-ii) and Figure 6(b-ii) are confined to either the first or third quadrants, with a positive slope. Substituting the expression $(\frac{-\theta\dot{s}_b}{\dot{s}})$ into Equation 36 results in a positive value for θ_{eff} , which is subsequently plotted in Figure 6(a-iii) and Figure 6(b-iii), yielding average values of 0.5213 and 1.1072, respectively.
- Additionally, the time history plots in Figure 6(c-i), Figure 6(d-i), and Figure 6(e-i) clearly demonstrate that the motion of the beam and the outer mass are out of phase. Consequently, the corresponding phase portrait diagrams in Figure 6(c-ii), Figure 6(d-ii), and Figure 6(e-ii) exhibit a negative slope. Substituting the expression $(\frac{-\theta\dot{s}_b}{\dot{s}})$ into Equation 36 results in a negative value for θ_{eff} . These values are plotted in Figure 6(c-iii), Figure 6(d-iii), and Figure 6(e-iii), with average values of -1.9462, -0.1826, and -0.1424, respectively.

5 Conclusions

This study introduces an algorithm based on the linear complementary problem (LCP), incorporating Euler's discretization, to analyze the dynamics of a novel metamaterial unit cell, where a cantilever beam functions as a resonator enclosed within an external mass. To validate the accuracy of the proposed computational approach, an experimental study has been carried out on the unit cell subjected to external excitation, with the results presented in this work. The transmittance outcomes derived from the theoretical model exhibit strong agreement with those obtained from experimental investigations. The successful validation of the proposed method reinforces its reliability for further analysis.

For the considered unit cell, the cantilever beam undergoes vibrations and impacts two rigid supports due to a pseudo force generated when the outer mass experiences external excitation. The developed LCP-based solver is further applied to assess the vibration attenuation characteristics of the metamaterial unit cell. The final LCP equation governing a single metamaterial unit cell reveals that its dynamic response is predominantly influenced by the mass ratio (θ), the inverse of the natural frequency of the outer mass (γ_s), the non-dimensional stiffness parameter (σ), and the non-dimensional normal gaps ($\tilde{g}_{N1}, \tilde{g}_{N2}$). To gain insight into the attenuation capability of the proposed unit cell, the transmittance spectrum is plotted for varying non-dimensional excitation frequencies across different values of the non-dimensional normal gaps. The out-of-phase motion between the vibrating beam and the outer mass results in a reduction in the displacement of the outer mass, thereby lowering the transmittance.

In addition to transmittance analysis, the effective mass of the metamaterial unit cell is also examined for different values of the non-dimensional excitation frequency (γ_r). A negative effective mass is observed for several values of γ_r , highlighting the potential of this unit cell in achieving effective vibration control.

References

1. Zapateiro, M., Karimi, H.R., Luo, N., Phillips, B.M., Spencer Jr, B.F.: Semiactive backstepping control for vibration reduction in a structure with magnetorheological damper subject to seismic motions. *Journal of Intelligent Material Systems and Structures* **20**(17), 2037–2053 (2009)
2. Adam, M., Von Estorff, O.: Reduction of train-induced building vibrations by using open and filled trenches. *Computers & Structures* **83**(1), 11–24 (2005)
3. Ye, L., Lu, X., Qu, Z., Hou, J.: Distributed tlds in rc floors and their vibration reduction efficiency. *Earthquake Engineering and Engineering Vibration* **7**(1), 107–112 (2008)
4. Samanta, A., Banerji, P.: Earthquake vibration control using sloshing liquid dampers in building structures. *Journal of Earthquake and Tsunami* **6**(01), 1250002 (2012)
5. Shum, K., Xu, Y.L.: Tuned liquid column dampers with adaptive tuning capacity for structural vibration control. *Structural engineering and mechanics: An international journal* **20**(5), 543–558 (2005)
6. Qiao, W.-T., Wang, D., An, Q., Zhang, H.-Y.: Study on dynamic behaviors and vibration reduction techniques on cable-supported ribbed beam composite slab. *ADVANCED STEEL CONSTRUCTION* **15**(1), 73–81 (2019)
7. Ghassempour, M., Failla, G., Arena, F.: Vibration mitigation in offshore wind turbines via tuned mass damper. *Engineering Structures* **183**, 610–636 (2019)
8. Chen, J., Han, Z., Xu, R.: Effects of human-induced load models on tuned mass damper in reducing floor vibration. *Advances in Structural Engineering* **22**(11), 2449–2463 (2019)
9. Qin, H., Yang, D.: Vibration reduction design method of metamaterials with negative poisson’s ratio. *Journal of Materials Science* **54**(22), 14038–14054 (2019)
10. Wu, X., Jin, Y., Khelif, A., Zhuang, X., Rabczuk, T., Djafari-Rouhani, B.: Topological surface wave metamaterials for robust vibration attenuation and energy harvesting. *Mechanics of Advanced Materials and Structures*, 1–9 (2021)
11. Stearns, A., Beck, B.: An optimization problem for maximum vibration suppression in reconfigurable one dimensional metamaterials. *New Journal of Physics* **23**(8), 083009 (2021)
12. Han, H., Sorokin, V., Tang, L., Cao, D.: Origami-based tunable mechanical memory metamaterial for vibration attenuation. *Mechanical Systems and Signal Processing* **188**, 110033 (2023)
13. Banerjee, A., Das, R., Calius, E.P.: Vibration transmission through an impacting mass-in-mass unit, an analytical investigation. *International Journal of Non-Linear Mechanics* **90**, 137–146 (2017)
14. Calius, E.P., Bremaud, X., Smith, B., Hall, A.: Negative mass sound shielding structures: Early results. *physica status solidi (b)* **246**(9), 2089–2097 (2009)
15. Banerjee, A., Das, R., Calius, E.P.: Frequency graded 1d metamaterials: A study on the attenuation bands. *Journal of Applied Physics* **122**(7), 075101 (2017)

16. Banerjee, A., Calius, E.P., Das, R.: An impact based mass-in-mass unit as a building block of wideband nonlinear resonating metamaterial. *International Journal of Non-Linear Mechanics* **101**, 8–15 (2018)
17. Hu, G., Tang, L., Banerjee, A., Das, R.: Metastructure with piezoelectric element for simultaneous vibration suppression and energy harvesting. *Journal of Vibration and Acoustics* **139**(1) (2017)
18. Pai, P.F., Peng, H.: Acoustic metamaterial structures based on multi-frequency vibration absorbers. In: *Health Monitoring of Structural and Biological Systems 2014*, vol. 9064, pp. 544–564 (2014). SPIE
19. Huang, H.-H., Sun, C.-T.: Anomalous wave propagation in a one-dimensional acoustic metamaterial having simultaneously negative mass density and young's modulus. *The Journal of the Acoustical Society of America* **132**(4), 2887–2895 (2012)
20. Pope, S., Laalej, H.: A multi-layer active elastic metamaterial with tuneable and simultaneously negative mass and stiffness. *Smart Materials and Structures* **23**(7), 075020 (2014)
21. Banerjee, A., Sethi, M., Manna, B.: Vibration transmission through the frictional mass-in-mass metamaterial: An analytical investigation. *International Journal of Non-Linear Mechanics* **144**, 104035 (2022)
22. Hussein, M.I., Leamy, M.J., Ruzzene, M.: Dynamics of phononic materials and structures: Historical origins, recent progress, and future outlook. *Applied Mechanics Reviews* **66**(4) (2014)
23. Huang, H., Sun, C., Huang, G.: On the negative effective mass density in acoustic metamaterials. *International Journal of Engineering Science* **47**(4), 610–617 (2009)
24. Liu, X.-N., Hu, G.-K., Huang, G.-L., Sun, C.-T.: An elastic metamaterial with simultaneously negative mass density and bulk modulus. *Applied physics letters* **98**(25), 251907 (2011)
25. Banerjee, A., Das, R., Calius, E.P.: A new approach for determination of the attenuation bandwidth of a resonating metamaterial. In: *Applied Mechanics and Materials*, vol. 846, pp. 264–269 (2016). Trans Tech Publ
26. Moreau, J.J.: Unilateral contact and dry friction in finite freedom dynamics. In: *Nonsmooth Mechanics and Applications* vol. 302, pp. 1–82. Springer, ??? (1988)
27. Panagiotopoulos, P.: Dynamic and incremental variational inequality principles, differential inclusions and their applications to co-existent phases problems. *Acta Mechanica* **40**(1-2), 85–107 (1981)
28. Panagiotopoulos, P.: Nonconvex energy functions. hemivariational inequalities and substationarity principles. *Acta Mechanica* **48**(3-4), 111–130 (1983)
29. Sethi, M., Banerjee, A., Manna, B.: Unilateral frictional contact between a rigid wheel traversing on a flexible beam: An analytical investigation. *Applied Mathematical Modelling* **120**, 612–635 (2023)
30. Banerjee, A., Chanda, A., Das, R.: Oblique frictional unilateral contacts perceived in curved bridges. *Nonlinear Dynamics* **85**, 2207–2231 (2016)
31. Rao, S.S.: *Vibration of Continuous Systems*. John Wiley & Sons, New Jersey (2019)
32. Alipour, A., Zareian, F.: Study rayleigh damping in structures; uncertainties and treatments. In: *the 14th World Conference on Earthquake Engineering*, pp. 12–17 (2008)
33. Cai, C., Zhou, J., Wang, K., Pan, H., Tan, D., Xu, D., Wen, G.: Flexural wave attenuation by metamaterial beam with compliant quasi-zero-stiffness resonators. *Mechanical Systems and Signal Processing* **174**, 109119 (2022)

34. Zhang, X., Li, Y., Wang, Y., Luo, Y.: Ultra-wide low-frequency bandgap design of acoustic metamaterial via multi-material topology optimization. *Composite Structures* **306**, 116584 (2023)
35. Aközbek, N., Mattiucci, N., Bloemer, M., Sanghadasa, M., D'Aguanno, G.: Manipulating the extraordinary acoustic transmission through metamaterial-based acoustic band gap structures. *Applied Physics Letters* **104**(16) (2014)